DAYSIDE PROTON AURORA: COMPARISONS BETWEEN GLOBAL MHD SIMULATIONS AND IMAGE OBSERVATIONS

J. BERCHEM[1], S.A. FUSELIER[2], S. PETRINEC[2], H.U. FREY[3] and J.L. BURCH[4]

[1] *Institute of Geophysics and Planetary Physics, University of California, Los Angeles, CA, USA*

[2] *Lockheed Martin Advanced Technology Center, Palo Alto, CA, USA*

[3] *Space Sciences Laboratory, University of California, Berkeley, CA, USA*

[4] *Southwest Research Institute, San Antonio, TX, USA*

Abstract. The IMAGE mission provides a unique opportunity to evaluate the accuracy of current global models of the solar wind interaction with the Earth's magnetosphere. In particular, images of proton auroras from the Far Ultraviolet Instrument (FUV) onboard the IMAGE spacecraft are well suited to support investigations of the response of the Earth's magnetosphere to interplanetary disturbances. Accordingly, we have modeled two events that occurred on June 8 and July 28, 2000, using plasma and magnetic field parameters measured upstream of the bow shock as input to three-dimensional magnetohydrodynamic (MHD) simulations. This paper begins with a discussion of images of proton auroras from the FUV SI-12 instrument in comparison with the simulation results. The comparison showed a very good agreement between intensifications in the auroral emissions measured by FUV SI-12 and the enhancement of plasma flows into the dayside ionosphere predicted by the global simulations. Subsequently, the IMAGE observations are analyzed in the context of the dayside magnetosphere's topological changes in magnetic field and plasma flows inferred from the simulation results. Finding include that the global dynamics of the auroral proton precipitation patterns observed by IMAGE are consistent with magnetic field reconnection occurring as a continuous process while the IMF changes in direction and the solar wind dynamic pressure varies. The global simulations also indicate that some of the transient patterns observed by IMAGE are consistent with sporadic reconnection processes. Global merging patterns found in the simulations agree with the antiparallel merging model, though locally component merging might broaden the merging region, especially in the region where shocked solar wind discontinuities first reach the magnetopause. Finally, the simulations predict the accretion of plasma near the bow shock in the regions threaded by newly open field lines on which plasma flows into the dayside ionosphere are enhanced. Overall the results of these initial comparisons between global MHD simulation results and IMAGE observations emphasize the interplay between reconnection and dynamic pressure processes at the dayside magnetopause, as well as the intricate connection between the bow shock and the auroral region.

1. Introduction

Recent model refinements and computational advances allow direct comparison of observations with results from global magnetohydrodynamic (MHD) simulations of the time-dependent interaction of the solar wind with the Earth's magnetosphere. In these studies, solar wind plasma and magnetic field measurements are used as input parameters to drive the simulations. Results from the simulations are then compared with observations in the magnetosphere. To date most of such compar-

isons have focused on the structure and dynamics of the magnetotail and nightside auroral activity. Early studies investigated the growth phase and expansion onset of substorms (Fedder *et al.*, 1995), large-scale flows of cold and dense ions in the distant tail (Frank *et al.*, 1995), the boundary layer formation in the magneto-tail (Raeder *et al.*, 1997), the response of the distant magnetotail to the east-west component of the interplanetary magnetic field (IMF) (Berchem *et al.*, 1998a), the auroral brightening and the onset of lobe reconnection during an isolated substorm (Lyon *et al.*, 1998), the response of the polar cap and high-latitude convection to a sudden southward turning of the IMF (Lopez *et al.*, 1998), and pseudobreakups and substorm onsets (Pulkinnen *et al.*, 1998; Slinker *et al.*, 2001). More recently global MHD simulations were used to model the spectacular interaction of the Earth's magnetosphere (Goodrich *et al.*, 1998) with a magnetic cloud driven by a coronal mass ejection (CME) (e.g. Fox *et al.*, 1998), the magnetotail dynamics during the December 10, 1996 storm, and the extreme compression of the magnetosphere that occurred on May 4, 1998 (Berchem *et al.*, 2001a). The over-all good agreement found in those studies between simulation results and both *in-situ* and ground measurements confirmed the validity of the approach.

While most of the studies have focused on the nightside, the use of global MHD simulations to study dayside magnetospheric processes offers numerous advantages. This is because the interaction between the solar wind and the dayside magnetosphere is more direct than the interaction in the magnetotail. Furthermore, the magnetic field-line mapping to the ionosphere is not as complex as that for the nightside. Recent investigations of the dayside magnetospheric boundary using global simulations include studies of a series of magnetopause crossings ("skimming" events) observed by the GEOTAIL spacecraft (Berchem *et al.*, 1998b) and the CLUSTER spacecraft (Berchem *et al.*, 2001b). These simulations addressed the complex topology of the magnetic field draping and reconnection patterns that can occur at the dayside magnetopause for periods of northward IMF with strong B_X and B_Y components and also address the effects of solar wind pressure pulses. Other dayside simulations focused on the displacement of the cusps resulting from changes in solar wind dynamic pressure and IMF orientation (Escoubet *et al.*, 1997; 1998). The results of these simulations are in very good agreement with results from previous statistical studies of low-altitude observations (e.g., Cabary and Meng, 1986; Woch and Lundin, 1992; Newell and Meng, 1995). In particular, simulation results confirm that the invariant latitudes of the polar and equatorial boundaries of the cusp depend significantly more on the value of the IMF B_Z than on the solar wind dynamic pressure (Escoubet *et al.*, 1998). Ionospheric convection patterns computed from global MHD simulations have also been compared with results using the AMIE technique (Richmond and Kamide, 1998) for several events (Raeder *et al.*, 1998; Slinker *et al.*, 1999). Very recently, another comparison between a global simulation and POLAR spacecraft *in-situ* ion measurements in the dayside magnetosphere demonstrated the connection between the cusps and the magnetopause/bowshock (Fuselier *et al.*, 2002a).

Despite the global nature of the simulations, most of the previous comparison studies of the dayside magnetosphere were carried out using time series from single and multipoint measurements. This paper takes comparison studies to a new level by using global observations of proton precipitation in the dayside ionosphere. Specifically we compare images from the FUV SI-12 instrument onboard the IMAGE spacecraft with the patterns of plasma flow into the ionosphere, as calculated from the global simulations. Results from the simulations allow us to investigate the response of the dayside magnetosphere to changes in dynamic pressure in the solar wind as well as changes in the IMF orientation. In particular, tracing magnetic field lines and using the enhancement of plasma beta as a diagnostic of magnetic field reconnection allow us to reconstruct the topology of the merging regions and its time evolution during the interaction of the solar wind with the dayside magnetosphere. The determination of the merging topology of the dayside magnetosphere and its dynamics is one of the foremost outstanding problems of magnetospheric physics. It is of special interest because of its potential for gaining an understanding of the morphology of the magnetosheath boundary layer and the cusp, and particle precipitation patterns (see Onsager *et al.* (2001) and Wing *et al.* (2001), and references therein) because phenomenological models depend strongly on the merging geometry they assume, i.e. antiparallel merging (Crooker, 1979) or component merging (e.g., Cowley, 1973). For example, determining the merging topology to be used in conjunction with observation-based magnetic field models (e.g., Tsyganenko, 1995) is a critical element for studying kinetic aspects of the cusp dynamics and ionospheric outflow, which can not be addressed by a single fluid MHD model (e.g., Fuselier *et al.*, 2002c; Petrinec *et al.*, 2002).

Section 2 briefly describes the global model and the simulation setup. Section 3 presents the first of the paper's two comparisons between images of proton auroras from the FUV SI-12 instrument onboard the IMAGE spacecraft, and the results of global MHD simulations. After a brief description of the magnetic field and plasma parameters measured by the WIND spacecraft on June 8, 2000, we compare images from the FUV SI-12 instrument with the patterns of plasma flow into the ionosphere, as calculated from the global simulations. Section 4 presents a second comparison involving images of auroral emissions from July 28, 2000. Next, in Section 5, we use isosurfaces of the plasma beta and field-line tracings from the simulations to establish relationships between downward flow patterns and the occurrence of magnetic field reconnection. We discuss the results of the comparisons and the global configurations of the dayside magnetosphere inferred from the simulations in Section 6 and examine the topology of the merging regions found in the simulations in the context of the antiparallel and component merging models. Section 7 concludes the paper with a summary of results.

2. Simulation model

The magnetospheric part of the simulation model used in our study is based on a single fluid MHD description (e.g., Berchem *et al.*, 1995a, b; Raeder *et al.*, 1995). Although diffusion and viscosity arise when the ideal MHD equations are solved numerically, the use of an explicit conservative predictor-corrector scheme for time stepping and hybridized numerical fluxes for spatial finite differencing constrains the numerical resistivity to a very low level. The small amount of dissipation produced by the algorithm prompted the retention of the resistive term (ηj) in Ohm's law ($\mathbf{E} = -\mathbf{v} \times \mathbf{B} + \eta j$) to produce the reconnection rates expected for the magnetic merging occurring in the magnetosphere. The resistivity η used in the model is a nonlinear function of the local current density j such that $\eta = \alpha j^2$, where α is an empirically determined parameter ($\alpha \ll 1$). In addition, a threshold is included in the model to avoid spurious dissipation. This threshold is a function of the local normalized current density and has been calibrated such that the resistivity term (ηj) is switched on at only a very a few grid points in strong neutral sheets (Raeder *et al.*, 1996). Similar phenomenological resistivity models have been used in local MHD simulation models (e.g., Sato and Hayashi, 1979; Ugai, 1985) and are based on the assumption that current-driven instabilities are responsible for the anomalous resistivity that produces reconnection. Since both threshold and resistivity depend on the local current density, the resistivity model enhances the occurrence of reconnection for large shear angles of the magnetic field; this is a significant consequence.

Boundary conditions are important features of the global model. To determine the ionospheric boundary of the model, a spherical shell with a radius of 2.7 R_E is placed around the Earth. This shell excludes the region where the Alfvén velocity becomes too large to be used in determining the simulation's time step. Inside the shell, the MHD equations are not solved, and a static dipole magnetic field is assumed to map the field-aligned currents from the shell boundary to the ionosphere. The model assumes a two-dimensional ionosphere to close the field-aligned currents and to solve the ionospheric potential equation to determine the electrostatic potential self-consistently. A proxy of three ionization sources (solar EUV ionization, precipitating electrons, and diffuse electron precipitation) is used to compute the ionospheric Hall and Pedersen conductances required to solve the potential equation (Raeder *et al.*, 1996). Once the ionospheric potential is determined, it is mapped to the spherical shell, where it is used as a boundary condition for the magnetospheric flow velocity.

Values of the solar wind plasma parameters (density, temperature, and velocity) and the IMF are imposed on the sunward face of the simulation system. Open boundary conditions ($\partial/\partial n = 0$) are assumed for all of the other sides of the simulation box ($320 \times 50 \times 50$ R_E). Actual one-minute averaged data from the WIND or ACE spacecraft located upstream of the bow shock were used to determine the inflow boundary conditions of the simulations presented in this paper. The simula-

tion runs were initialized by switching on the input solar wind flow between two and three hours before the time intervals examined in the study (June 8 and July 28, 2000). These periods for preconditioning the simulations are longer than the times required for the solar wind to convect through the entire system used, which are about seventy-five minutes and two hours for the June 8 and July 28 cases, respectively. These periods give the simulation system time to evolve towards a physical state that is independent of the initial conditions.

Both the solar wind magnetic field and the plasma parameters must be advected from the spacecraft location to the inflow boundary of the simulation box, located 20 R_E in front of the Earth, before being used as input to the simulation. However, because solar wind measurements are available for only a single location, several assumptions were made in the process. The first assumption is that the solar wind plasma is not affected by any dispersion or steepening as it convects from the spacecraft location where it is measured to the simulation's boundary. Previous studies using ACE and WIND spacecraft measurements in combination with observations from the magnetosheath indicate this assumption is valid most of the time (e.g., Berchem *et al.*, 2001a). However, it is not unusual to find large discrepancies between measurements from different solar wind monitors. Solar disturbances have complex geometries and, as they expand, they interact with the interplanetary medium. Numerous discontinuities present in the solar wind as it moves away from the Sun fail to reach the magnetosphere or are significantly altered during their convection from the sunward Lagrangian point (L1) to the Earth (Collier *et al.*, 1998). Hence, it is necessary to compare simulation results with observations before attempting any interpretation of their results.

The second assumption made in setting up the simulations concerns the IMF input. While actual plasma measurements from the solar wind monitors were used, magnetic field data required some processing to make them usable. This is because Faraday's law prevents the advection of fluctuations along the B_X component at the inflow boundary of our simulation system. To obviate that difficulty, the strongest variations of the solar wind magnetic field were assumed to lie in parallel planes. This assumption allowed us to use minimum-variance analysis over the entire data interval to determine the average normal direction of the magnetic field fluctuations. Magnetic field data were then transformed from the geocentric solar ecliptic (GSE) system to the new system, which was determined by the normal direction and the two other eigenvectors. The next steps were to set the magnetic field component along the normal to equal the magnitude of the average field along that direction and to transform the magnetic field to the simulation's system of coordinates (GSE) before propagating the field to the inflow boundary. Results of the transformations for the two time intervals used in the study show only small deviations from the actual IMF measurements, indicating that the assumptions made regarding the structure of the solar wind fluctuations during the time interval considered were reasonable.
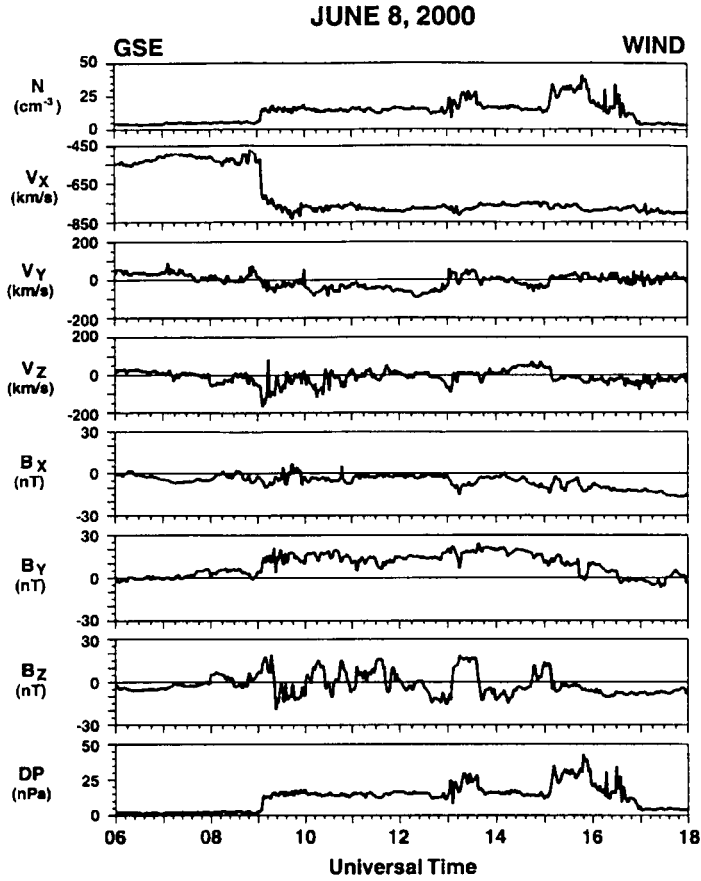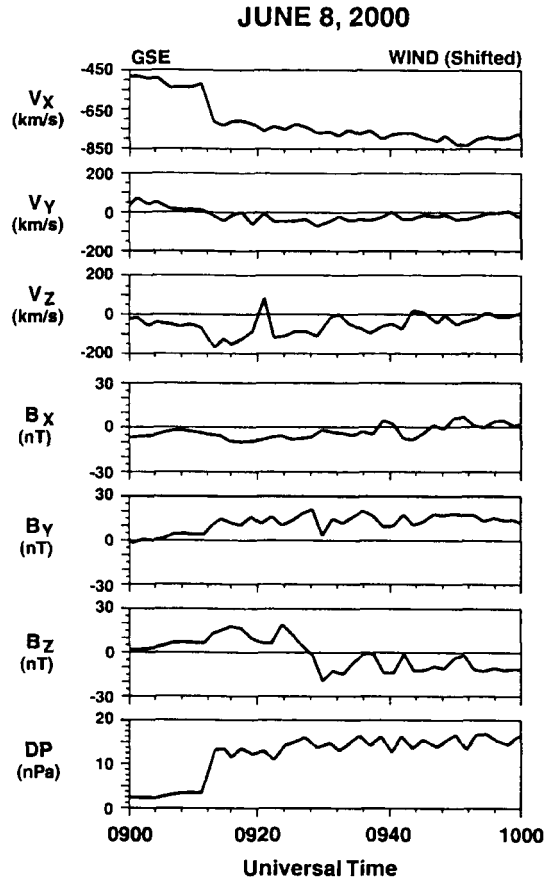
JUNE 8, 2000

Figure 1. Plasma and field parameters measured by the WIND spacecraft during 0600-1800 UT on June, 8, 2000, and plotted using the GSE system of coordinates. From top to bottom are shown the ion density per cm^3, the three components of the bulk velocity in km/s, the three components of the magnetic field in nanotesla, and the dynamic pressure in nanopascal.

3. June 8, 2000

The first event examined in this paper occurred on June 8, 2000. WIND ion measurements and magnetic field components from 0600 UT to 1800 UT are shown in Figure 1. The data are one-minute averaged and displayed in Earth-centered solar ecliptic (GSE) coordinates. The remainder of this paper uses the GSE coordinate for spacecraft locations and in the observations and simulation results. At 0900 UT the WIND spacecraft was located at $R_W = (40.7, -26.4, -4.3)$ R_E. Figure 1 displays from top to bottom, the ion density in particles per cm^3, the three components of the ion bulk velocity in km/s (Ogilvie *et al.*, 1995), and the three components

JUNE 8, 2000

Figure 2. Plasma and field parameters measured by the WIND spacecraft shifted by 7 min. and plotted in GSE coordinates from 0900 to 1000 UT on June, 8, 2000. From top to bottom are shown the three components of the bulk velocity in km/s, the three components of the magnetic field in nanotesla, and the dynamic pressure in nanopascal.

of the magnetic field in nT from the GSFC magnetometer (Lepping *et al.*, 1995). The bottom panel shows the dynamic pressure calculated from the ion density and the bulk speed of the solar wind. The WIND measurements show the progression of a strong solar disturbance toward Earth, as indicated by the enhancement of the dynamic pressure between 0900 UT and 1700 UT. The strong interplanetary shock observed at about 0906 UT marks the leading edge of the disturbance, suggesting that it is probably a coronal mass ejection (CME). The foreward shock is readily identified in the ion measurements by a large density enhancement from about 5 to 15 particles per cm^{-3} and a sharp jump in bulk velocity from about 550 km/s to 750 km/s. An increase in the IMF magnitude, from about 6 to 21 nT, occurs simul-
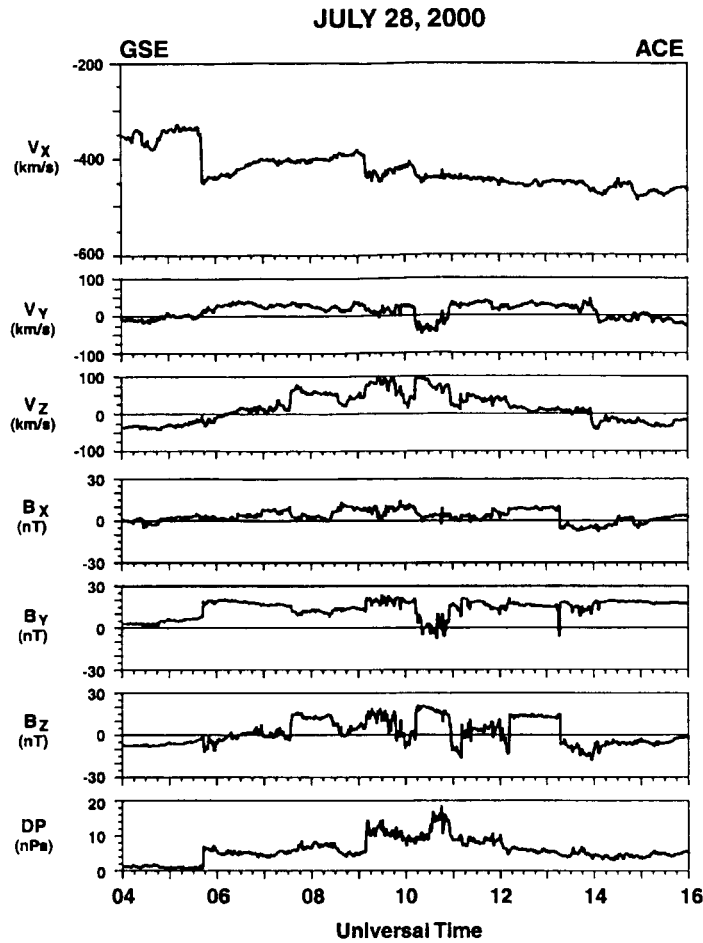
JULY 28, 2000

Figure 3. Plasma and field parameters measured by the ACE spacecraft during 0400–1600 UT on July, 28, 2000 and plotted using the GSE system of coordinates. From top to bottom are shown the three components of the bulk velocity in km/s, the three components of the magnetic field in nanotesla, and the dynamic pressure in nanopascal.

taneously. The solar wind dynamic pressure remains high throughout the 8 hours following the initial shock. This interval is characterized by a long period, from about 0900 to 1300 UT, when the dynamic pressure is nearly constant (15 nPa) followed by several large pressure enhancements with peaks between 25 and 40 nPa. These fluctuations result from large enhancements in the plasma density rather than in the bulk velocity of the plasma, indicating the presence of large-scale structures in the solar stream that are not shocks. The IMF fluctuates markedly through out the entire time interval, but most of the large-amplitude fluctuations occur along

the Z-component, while the Y component of the field remains duskward with a more or less constant magnitude of about 16 nT.

In this section we compare our simulation results to remote sensing observations of the proton aurora. These images are from the Spectrographic Imager (SI-12), one of the three imagers of the Far Ultra-Violet (FUV) experiment (Mende *et al.*, 2000) onboard the Imager for Magnetopause to Auroral Global Exploration (IMAGE) spacecraft (Burch, 2000). The FUV SI-12 instrument images precipitating protons using emissions centered on 121.8 nm. These emissions occur when energetic protons collide with atoms and molecules in the upper atmosphere. During some of the collisions, protons undergo charge exchange by capturing electrons, leaving fast hydrogen atoms excited in the upper state of the Lyman alpha (Ly-α) transition. Line profiles and Doppler shifts of the photons emitted by the hydrogen atoms depend in a complex way on the initial energies and pitch angle distributions of the precipitated protons. Though the FUV SI-12 imager does not allow the exact determination of Doppler shifts, theoretical models indicate that emissions around 121.8 nm correspond to precipitating protons with initial energies of 2–8 keV (Gérard *et al.*, 2000). Since magnetosheath protons that precipitate in the cusp typically have energies of 1 keV, only energetic protons observed during periods of enhanced solar wind dynamic pressure produce emissions that are strong enough to be measured by the FUV SI-12 instrument (e.g., Fuselier *et al.*, 2001). This is the reason our comparison study focuses on two events that occurred during periods of enhanced solar wind dynamic pressure. Another important reason to focus on events such as that of June 8, 2000, is that the time delay between the observation of the dynamic pressure change by the solar wind monitor and the arrival of the pulse in the ionosphere can be determined unambiguously from the observations.

We begin by describing the format used in Plates 1 and 2 to present the comparison of simulation results with images from the FUV SI-12 instrument. The left panels of Plates 1 and 2 show the color contours of the corrected counts (flat-fielded and corrected for temporal variation in instrument sensitivity) from FUV SI-12 displayed in magnetic latitude and magnetic local-time coordinates. The right panels show in the same coordinate system, color contours of plasma flows into the ionosphere, as predicted by the global MHD simulation. The latitude range displayed extends down to 50°, though the cutoff imposed by the inner boundary is around 62°. Downward flows are obtained by calculating the earthward component of the bulk flow's velocity that is parallel to the magnetic field ($V_{\parallel}$) at the inner boundary shell of the simulation system. This component is then mapped to the ionosphere using a model of Earth's dipole magnetic field. Both northern and southern auroral regions are displayed. As we discuss below, these synoptic views reveal that, very often, solar disturbances result in significant differences between the downward flow patterns occurring in the southern and northern auroral regions. Both ionospheric displays are viewed from above the Northern Hemisphere, and hence noon is at the top and dusk is on the left in both views. Although it takes the FUV SI-12 instrument about 10 s. to produce an image, the 2-min. spin period of

the spacecraft determines the image cadence. Since the simulations' time steps and sampling rates used to input the solar wind data are smaller than the image cadence, it is straightforward to match the simulation output with FUV measurements. However, it is necessary to set the time delay between the observation of the stream by the solar wind monitors and its arrival at the upstream boundary of the simulation. As mentioned in the brief description of the simulation model, this is achieved by assuming a very ballistic model of the solar wind propagation. The occurrence of interplanetary shocks and dynamic pressure pulses made it straightforward to assess the validity of this assumption for the events considered in this study. In this case and in the 28 July case discussed below, the times determined by this method were correct within the 2-min. uncertainty between each FUV SI-12 image.

When comparing FUV SI-12 images of proton auroras with results from the global simulations, it is important to remember that only activity enhancements observed in the dayside of the auroral region should be considered. As we show below, our comparison is based on the simple assumption that enhancements of ion precipitation in the dayside auroral region coincide with the increase of downward flows along dayside reconnected field lines, which are frequently observed in the simulations (e.g., Berchem *et al.*, 2001a). Because of the intricacy of magnetotail phenomena, such as the formation of the ring current by the injection of energetic particles during storm times, we do not expect such a simple diagnostic from the global simulation alone to reproduce the complex precipitation patterns observed in the nightside auroral region.

Plates 1 and 2 display downward flows from the global simulation and FUV SI-12 observations of proton auroras from 0910 to 0940 UT for June 8, 2000. As the spacecraft descended from apogee, the instrument had only a slanted view of the northern auroral oval, instead of an optimal nadir view. Furthermore, the observations shown were taken early in the mission, before FUV SI-12 instrument settings were optimized. Therefore, auroral structures appear smeared from the top right to the bottom left of the images. Instrument settings and observation conditions were much better on July 28, 2000, the event shown in Plates 3 and 4. Both Plates 1 and 2 are made up of individual panels that use the format described above to display the results. The panels are about 2 min. apart (FUV's sampling rate) and organized sequentially into two columns, with the earliest time displayed in the upper left corner of each plate. Figure 2 shows an enlargement of Figure 1 in which the solar wind parameters displayed have been shifted by about 7 min. to take into account the propagation time from the WIND spacecraft.

The first panel in Plate 1 shows the auroral region at 0910 UT, just before the initial impact of the interplanetary shock with the magnetosphere. In both the spacecraft data and the simulation results only faint spots are perceptible. At 0912 UT the effects of the interplanetary shock's collision with the magnetopause are clearly seen in the afternoon sector. FUV SI-12 observations show a strong enhancement of proton precipitation, marked by the formation of three bands between about 64° and 83° latitudes, the center one being located on the auroral oval (Fuse-

lier *et al.*, 2002b). The simulation shows strong enhancement of the downward flows poleward of the auroral oval, though with fewer apparent structures. An additional feature revealed by the simulation is that the interplanetary shock affects a much wider range of local times in the auroral region of the Southern Hemisphere than of the Northern Hemisphere. The associated IMF orientation is slightly northward and duskward. Two minutes later, at 0914 UT, a strong enhancement persists in both the observations and the simulation results. However, the area with the most intense precipitation has moved toward the terminator and has been reduced considerably in size. This new spot is located around 73° latitude in the dusk sector and seems to emanate from the center of the earlier three-banded structure, which is still perceptible in the afternoon sector of the FUV SI-12 image. It is interesting that the duskward displacement of the precipitation coincides with the small rotation of the IMF clock angle indicated by increases in both the B_Z and the B_Y components. From that time until 0928 UT, precipitation gradually fades away while the spot's location oscillates around the late afternoon sector, though there is a brief intensification around 0922 UT. During that period the associated IMF and dynamic pressure also change (see Figure 2).

Around 0928 UT (Plate 2) the field starts to turn southward, and a small enhancement in the solar wind dynamic pressure occurs. FUV SI-12 images indicate that the location of maximum precipitation has moved sunward and is now centered on the noon sector and encompasses a wide range of latitudes. The simulation also shows enhanced precipitation in the noon sector, but the enhancement is less intense than the one observed by FUV SI-12, though this could be an artifact of the different scale and color scheme used in the simulation. The most striking feature shown by the simulation is the formation of a wedge pattern. This feature does not occur in the observations for that time frame, but in the next one, at 0930 UT, a two-banded feature is clearly evident. This pattern is somewhat reminiscent of the large structure that formed during the initial interaction with the interplanetary shock at 0912 UT. However, the band observed below the auroral oval is now absent. The corresponding snapshot from the simulation for time 0912 UT shows a pattern and a level of enhancement very similar to those observed by the SI-12 instrument. In addition, it is important to note that the excursion of the enhanced precipitation into the prenoon sector, observed between 0928 UT and 0930 UT, occurs around the time of a short drop in the B_Y component of the lagged IMF, i.e. a rotation of the clock angle to a more southward direction.

After 0930 UT, the B_Y component recovers its previous value and stays fairly constant until the end of the period displayed in Plates 1 and 2 (0940 UT). It is interesting that the enhanced precipitation returns to its initial location in the afternoon sector, and observations show that it remains predominantly in that region for the rest of the sequence. While the longitudinal position of the cusp precipitation is controlled by B_Y, the B_Z component controls its latitudinal position. It is clear that during the entire period following the southward turning of the IMF, the enhanced precipitation region occurs at lower latitudes than during the period of northward

IMF. The simulation shows a similar correlation between the displacement of enhanced downward flows and the direction of the IMF. However, there is a clear drop in the intensity of the flows when the IMF turns duskward ($B_Z \approx 0$) for a short time period around 0938 UT that is not seen in the observations. In addition, the simulation indicates strong enhancement of precipitation in the Southern Hemisphere during periods of southward IMF.

4. July 28, 2000

Figure 3 shows a time series of the solar wind ions and magnetic field measured by the ACE spacecraft for the second event of the study from July 28, 2000. Data are shown for the period 0400 to 1600 UT in GSE coordinates. From top to bottom are displayed the three components of the ion velocity from the ACE/SWEPAM experiment (McComas *et al.*, 1998), the three components of the magnetic field from the ACE/MAG instrument (Smith *et al.*, 1998), and the ion dynamic pressure. At 1100 UT the ACE spacecraft was located at $R_A = (249.9, 1.8, 21.9)$ R_E. The large enhancement of the solar wind dynamic pressure seen in Figure 3 is similar to that of the June 8, 2000 event (Figure 1). Clear jumps in the ion parameters and the magnetic field measurements at 0543 UT mark the beginning of the disturbance. The ion density and the field magnitude jumps, from about 5 to 17 particles per cm^{-3} and from about 8 to 20 nT, respectively, are very close to those measured on June 8. However, the initial bulk velocity (about 340 km/s) and the velocity jump (about 100 km/s) are not as large as those observed in the June 8 event. As a result, the dynamic pressure of the solar disturbance (about 8 nPa) is barely half of that observed on June 8. Nevertheless, the stream also appears to include large-scale structures with several pressure peaks above 15 nPa. The magnetic field of the solar disturbance observed on July 28 also shows some similarities to the June 8 case. Most of the IMF fluctuations occur along the Z-component, and the field has a strong duskward component (IMF $B_Y > 0$). However, unlike the June 8 event, in the July 28 event the IMF B_Y component oscillated around zero even during a short period between 1015 and 1100 UT.

The results of our second comparison are shown in Plates 3 and 4. The interval considered is the period from 1151 to 1222 UT on July 28, 2000. FUV SI-12 images and simulation snapshots are displayed in individual panels using a format similar to the one used for Plates 1 and 2. As in Plates 1 and 2, the panels are about 2 min. apart and organized sequentially into two columns, with the earliest time displayed in the upper left corner of each plate. The main features of this time period are two clear changes in the IMF orientation. The first is a slow rotation of the field from north to south that takes place between 1151 and 1214 UT, while the second change is much faster, occurring between 1214 and 1216 UT when the IMF retraces part of the previous rotation.

AUTHOR, NEW ART WORK PLEASE

Figure 4. Plasma and field parameters measured by the ACE spacecraft shifted by 63 min. and plotted in GSE coordinates from 1100–1300 UT on July 28, 2000. From top to bottom are shown the three components of the bulk velocity in km/s, the three components of the magnetic field in nanotesla, and the dynamic pressure in nanopascal

Figure 4 displays the solar wind magnetic field and dynamic pressure shown in Figure 3 for that time interval, but shifted by about 63 min. to take into account the propagation time from the ACE spacecraft. From 1151 to 1157 UT, FUV SI-12 observations show a weak precipitation pattern that fades away as the IMF rotates from north to dusk. Although faint, a two-banded structure in the form of a wedge is perceptible in the afternoon sector. Previous time frames (not shown) indicate that this structure was present earlier, and thus it is probably associated with the previous IMF configuration. The simulation faithfully reproduces both the fading of the emissions and the formation of a wedge-like structure. However, the simulation shows a more localized and stronger enhancement of the flows in the poleward branch of that structure than is seen in the FUV SI-12 images. Nonetheless, these strong flows die out around 1157 UT, in agreement with the observations.

At 1159 UT, the IMF is still rotating and begins to develop a significant B_Y component. FUV SI-12 images from that time frame show the growth of two spots in the noon and afternoon sectors at two different latitudes. At 1201 UT, the poleward spot has moved toward noon and merged with the lower spot to form a single larger one. In the subsequent images (1203–1210 UT) the emissions intensify while broadening in longitude and moving toward lower latitudes as the field turns more and more southward. After a period of strong enhancement during

the relatively steady IMF from 1208 to 1212 UT, precipitation begins to fade as the field turns duskward (1216 UT). FUV SI-12 images indicate that at 1218 UT the maximum precipitation is located in the afternoon sector. From that time until the end of the sequence at 1222 UT, observed precipitation moves gradually and slightly duskward. The intensity of the emissions weakens considerably as the solar wind dynamic pressure drops. The simulation results from the period 1159 UT to 1222 UT clearly confirm that the model accurately reproduces the displacement of the precipitation enhancement toward lower latitudes as the IMF turns south (1159–1203 UT). Downward flows from the simulation are also in good agreement with the intensification of the proton precipitation observed by FUV SI-12 and with the broadening of the region during the period of southward IMF (1208–1214 UT). It is interesting that for the July 8 case, the simulation predicts a strong enhancement of precipitation in the Southern Hemisphere for periods of southward IMF. Finally, the simulation also reproduces the duskward displacement of the emissions as the IMF turns duskward in the last phase of the sequence (1210–1222 UT).

Altogether the two comparisons presented above of the FUV SI-12 images with the results of global MHD simulations show a remarkable degree of agreement between the observed proton auroras and the downward flows calculated from the simulations. In particular, the simulation confirms the strong dependence of the location of the proton emissions on the direction of the IMF. It is clear from the FUV SI-12 observations that the emissions from proton precipitation move poleward when the IMF turns northward and equatorward when the field turns southward, whereas their azimuthal displacement is determined by the direction of the IMF's B_Y component. It is also evident that the position of emissions covers a wide range of local time with a narrow latitudinal spread around the auroral oval for southward IMF, whereas for northward IMF they are highly focused near local noon and cover a larger range of latitudes. Although this study considers only ions, the observations and simulation results are fully consistent with both previous *in-situ* measurements and earlier ground observations of particle precipitation. Since Burch (1972) first identified the dependence of the magnetospheric cusp location on the magnitude of the B_Z component of the IMF, numerous observational studies have investigated the response of the cusp to changes in solar wind. It is now well established that the IMF orientation and solar wind dynamic pressure exert a strong influence on the structure and dynamics of the cusp (e.g., Burch *et al.*, 1985; Carbary and Meng, 1986; Newell and Meng, 1988; Newell *et al.*, 1989; Woch and Lundin, 1992; Wing *et al.*, 2001). In particular, observations and simulation results agree with the observed energy-dispersion dependence of injected ions on IMF B_Z, which is related to considerations of time-of-flight effects on newly reconnected field lines (e.g., Onsager *et al.*, 1993; Woch and Lundin, 1992; Smith and Lockwood, 1996). The dependence of the precipitation patterns on IMF B_Y is also consistent with results of previous studies of auroral dynamics and dayside convection for an IMF with a predominantly positive B_Z component but a varying B_Y (Milan *et al.*, 2000). The dependence is also in accord with recent observations of proton auroras in the cusp

by the FUV SI-12 (Frey *et al.*, 2002). Below, we address these dependences in a discussion of indications of dayside merging in the simulations.

Another interesting feature revealed by the comparisons is an enhanced dependence of the precipitation's intensity on the solar wind dynamic pressure. The expansion of the cusps' footprints as the solar dynamic pressure increases has been studied using both statistical observations at low altitudes (Newell and Meng, 1995) and results from global simulations (Escoubet *et al.*, 1997; 1998). A dependence of the brightness of the proton precipitation on the solar wind dynamic pressure is also observed in FUV SI-12 images of proton auroras in the cusp (Frey *et al.*, 2002). This dependence on solar wind dynamic pressure is obvious during the interaction with the interplanetary shock observed on June 8 (Plate 1). On a smaller scale, dependence on solar wind dynamic pressure appears to explain some of the variability in the precipitation's intensity during short periods of quasi-steady IMF. Nevertheless it is hard to ascertain the existence of such dependence because of the difficulty in determining exactly the timing of small pressure changes in the solar wind data. Similar uncertainties encountered in trying to find precise matches of individual features seen in the data with the simulation results. However, some of these small discrepancies can be resolved by slightly delaying or advancing in time the simulation results to achieve a better match with the observations.

In summary, we found very good agreement between intensifications in the auroral emissions measured by the FUV SI-12 instrument and the enhancement of downward plasma flows predicted by global MHD simulations. In particular, the simulations reproduce very well the displacements of auroral emissions that occur in response to changes in the orientation of the IMF. Nonetheless, there are some discrepancies between observations and simulation results. Small inconsistencies may plausibly result from small changes in the solar wind occurring during its propagation from L1 to Earth. The model itself rather than the input may cause another type of discrepancy between simulations and observations. A prime example of this is the absence in the simulation of the band at the lowest latitudes immediately after the impact of the interplanetary shock. Recently Fuselier *et al.* (2002b) suggested that this feature could result from ring-current emissions stimulated by the interplanetary shock. Since our model does not include a ring current, its absence from the simulation could, in fact, indirectly support this hypothesis.

5. Magnetic field topology of the dayside magnetosphere

The good agreement found between the IMAGE observations and the results from the global MHD simulations validates the use of the simulations to investigate the topological changes of the dayside magnetosphere revealed by proton auroral emissions. In the discussion below we focus on two aspects of this process. First, we examine the large-scale auroral structures created by the June 8, 2000 interplanetary shock. Because of the intensity and rapidity of the interaction, these structures

provide clear signatures of transient processes resulting from changes in the IMF. In the second part of this section, we extend our analysis of the simulation results by using isosurfaces of plasma beta and field-line tracings to relate the evolution of auroral patterns to slower changes in the magnetic field configuration of the dayside magnetosphere. In particular, we examine a sequence that illustrates the changes that accompany a rotation of the IMF from North to South.

Plates 5 and 6 show results of the June 8, 2000, simulation for times 0911 and 0912 UT. They are snapshots taken just after the interplanetary shock collided with the dayside magnetopause. The (a) panels of Plates 5 and 6 show color-coded contours of the plasma flow velocity (V_Z) plotted in a cross-sectional plane taken at $Z = 4$ R_E and viewed from 1500 LT. Hence, dusk is on the right side, and the tip of the X-axis can be seen pointing toward the sun in the lower left corner of the picture. Color-contours have been restricted to a narrow range of velocities (± 50 km/s) to reveal the plasma flowing toward the ionosphere. The (b) panels use the same point of view as the (a) panels, but show only the field lines traced from the region of magnetospheric downward flows. Since the solar wind has a very strong southward velocity component (about 150 km/s) during that time interval, it appears as a solid red contour in the front of the figures. The 0911 UT snapshot (Plate 5) shows the initial compression of the entire dayside magnetosphere. The narrow arc of yellow and green contours delineates the dayside magnetosheath. The region of interest is the large red spot located in the subsolar region, earthward of the magnetopause boundary. It marks the occurrence of strong plasma flows directed toward the ionosphere. Tracing magnetic field lines from the periphery of that spot indicates that they are open field lines threading the cusp. The bends seen in the field lines (Panel b) indicate that these open field lines had been reconnected at high latitudes near the noon region LT of the Northern Hemisphere. They are connected to the upstream solar wind, crossing the bow shock in the afternoon sector of the Southern Hemisphere. This topology is consistent with the northward direction of the IMF just before and during the ramping of the magnetic field jump that marks the interplanetary shock (Figures 1 and 3). Plate 6 displays the simulation results for time 0912 UT. The fast magnetosonic wave launched by the collision of the transmitted shock with the magnetopause has propagated tailward. Red contours in the dawn and dusk regions indicate that the leading edge of the solar wind disturbance has reached the terminator. Subsolar bow shock and magnetopause boundaries are now more easily identified because of the strong upward flows (blue contours) seen in the magnetosheath, which are consistent with expectations for that region under normal conditions. The most striking development is that the large spot of downward flows seen at 0911 UT (red contours) is now divided into two bands. This is the magnetospheric counterpart of the ionospheric pattern seen in Plate 1.

Tracing field lines from the two bands shown in Panel (b) reveals that field lines threading the equatorward band have a topology very similar to that pictured in Plate 5 for time 0911 UT. However, although they are also reconnected to the upstream solar wind, the field lines threading the poleward band have a very dif-

ferent topology. The most poleward ones are markedly elongated in the east-west direction and intersect the $Z = 4 R_E$ plane at about 1800 LT, slightly tailward of the leading edge of the disturbance. It is very unlikely that field lines reconnected around noon LT could have been stretched and convected so far toward dusk (about $25 R_E$) during the 1-min. time that elapsed between the two snapshots. In addition, the bumps seen on the field lines at about $Y = 15 R_E$ show that they are being compressed by the fast magnetosonic wave, and pulled duskward from the afternoon region by the strong magnetosheath flow following the shock wave. These features indicate that the poleward band is threaded predominantly by field lines that were reconnected more recently than the open field lines shown in Plate 5. In contrast, the more equatorward patch seen in Plate 6 may plausibly be comprised by most of the open field lines observed earlier in Plate 5, which were stranded in the subsolar and postnoon regions. In the one-minute span between the two snapshots, these field lines have not been reconnected in the Southern Hemisphere to create new closed field lines. Because the interplanetary shock is marked by a jump in the B_Y and B_Z components of the IMF, the evolution of the field configuration seen in Plates 5 and 6 is consistent with the fast displacement of the merging region. As we show below it is also consistent with antiparallel merging. The fast process illustrated above is a good example of a transient response of the dayside magnetosphere that occurs faster than the 2-min. image cadence of the FUV SI-12 instrument. However, subsequent snapshots in Plate 1 show good agreement between the observed time evolution of the patterns and those predicted by the simulation.

Plates 7 and 8 show a sequence of simulation results from 0929 to 0935 UT for June 8, 2000, illustrating the effects of a slower change in the solar wind. Specifically, we focus on the effects of the turning of the IMF from North to South on the dayside magnetic field topology. One plate consists of three snapshots of the simulation results taken one minute apart. Each panel is composed of two subpanels showing ionospheric (right) and magnetospheric (left) results associated with the UT shown in the lower right corner. The format for displaying the flows toward the ionosphere (framed subpanel on the right) is identical to that used above to compare simulation results with IMAGE observations. The left subpanels are more complex. The picture displayed is a three-dimensional rendering of the dayside magnetosphere in GSE coordinates viewed from the sun (hence dusk is located on the right instead of the left in the ionospheric views). The background of the picture consists of a color contour plot of the plasma beta in a cross-sectional plane (Y-Z) taken at $X = -10 R_E$. Superimposed over these contours, a three-dimensional isosurface of plasma beta delineates regions of space bounded by a given value of the plasma beta. The same color scale is used as in the two-dimensional contours. Isosurfaces of plasma beta are used to diagnose the global topology of the magnetic field. Indeed, since variations of magnetospheric density are usually confined to a narrow range, the local enhancement of the plasma beta very often indicates a strong pinching of magnetic field lines. Regions of strong beta are primarily

observed in the magnetotail current sheet. In Plates 7 and 8, they appear as red contours in the dawn and dusk regions of the plasma sheet and as green contours near the equatorial plane. The plasma sheet itself is bounded by the deep blue contours delineating the magnetotail lobes. On the dayside magnetosphere, the magnetic field is strongly pinched where the IMF reconnects with the Earth's magnetic field. Thus the display of plasma beta isosurfaces can be used to visualize merging regions. Tracing actual field lines indicates that using isosurface values of around 10 is most successful for locating the occurrence of reconnection at the dayside magnetospheric boundary. These isosurfaces are color coded red. They roughly bound two wedge-shaped regions that extend from the magnetotail flanks to the front side, pointing more or less toward the subsolar region. It is important to note that merging occurs primarily in the narrow strips of the picture. Farther down the tail boundary, the high-beta regions indicated by the isosurfaces include field lines that are marked by sharp kinks resulting from reconnection at an upstream location. Most of these field lines are newly 'disconnected' field lines, i.e., both ends are in the solar wind, and have been dragged tailward by the magnetosheath flow. Depending on whether the IMF orientation is northward or southward, these fields lines either form a broad region of weak field that has been called the 'sash' (e.g., White *et al.*, 1998), or populate the flank boundary of the plasma sheet. Notice that the very coarse aspect of the isosurfaces is due to numerical artifacts in their computation. The last element of the picture shown in the left subpanels of Plates 7 and 8 is the display of field lines (yellow lines) threading the regions of downward flow toward the ionosphere and high-beta plasma. These field lines establish the relation between the magnetic field merging geometry and the auroral features displayed in the right subpanels of Plates 7 and 8.

The sequence shown in Plates 7 and 8 focuses on the effects of the southward turning of the IMF observed around 0931 UT when shifted in time to take into account its propagation from WIND's location (Figure 4). The sequence begins with a display of the results for time 0929 UT on day June 8, 2000 (Plate 7, top panel). Both B_Y and B_Z IMF components have positive values; however, B_Y is increasing while B_Z is decreasing. The auroral display shows the formation of two bands at different latitudes that converge toward noon LT. As seen in Plate 2, the structure appeared in the simulation following the decrease in B_Z that began a few minutes earlier. The two merging regions predicted by the simulation and shown by the red isosurfaces are positioned about 40° and 190° in clock angles with respect to the Z GSE axis. Although they are located at relatively high-latitudes in the GSE coordinate system, the merging regions are in fact closer to the magnetic equator than they appear to be because of the strong east-west inclination of the Earth's dipole (readily inferred from the direction of the tail lobes axis). One minute later (Plate 7, middle panel) the IMF B_Z is just about to turn South. Both merging regions have rotated about 10° toward the equatorial plane. The most striking feature of that motion is that the tips of the merging regions have extended to lower latitudes. A strong enhancement of the downward flow occurs simultaneously. The most

poleward of the two bands observed before has merged with the other band at a lower latitude to form a solid wedge with its tip on the noon meridian. It is clear that the auroral pattern follows the changes observed in the topology of the merging region.

At 0931 UT (Plate 7, bottom panel) the IMF is directed southward and has a small B_Y component resulting from a brief decrease in B_Y (see Figure 4). Both merging regions have spread sunward toward the subsolar region. They have also broadened significantly in latitude. Specifically, the northern branch now covers a wide range of latitudes in the dusk sector. Similar features are evident in the auroral plots. The enhancement of downward flows has moved equatorward to lower latitudes and spread markedly in local time toward dusk. It is interesting that the most poleward edge of the high-latitude band that was evident in the previous snapshots remains discernible. A two-band structure is also present in the IMAGE data (Plate 1), but at a slightly earlier time (0930 UT). However, because high-energy particles precipitate first, and because FUV SI-12 is more sensitive to high-energy protons, it is expected that high-energy protons make up most of the emissions observed by the instrument. Lower-energy protons precipitate later but have greater flux than the high-energy part of the distribution. They constitute most of the flows modeled by the MHD simulation, and therefore could explain the small time delay observed between the observations and the global MHD simulation. Yet it is not entirely clear whether the formation of simultaneous discrete structures results solely from flows coming from the higher-latitude region with lower energy, or instead indicates the persistence of reconnection at higher latitude, even as the IMF begins to merge at lower latitudes. Indeed, a simultaneous occurrence of reconnection at high and low latitudes has been postulated for conditions of a northward IMF and a significant B_Y component (Reiff and Burch, 1985). This interpretation seems consistent with the spread of the merging region indicated by the isosurfaces. In addition, time-of-flight effects could significantly amplify the formation of discrete flow patterns that result when merging occurs simultaneously at different latitudes. The occurrence of convection patterns involving simultaneous dayside and lobe reconnection was suggested by Weiss *et al.* (1995) to account for reversed ion dispersion seen by the DE 1 spacecraft in conjunction with strong westerly flows. More recently, Wing *et al.* (2001) suggested that double cusp structures in the ion dispersion observed by spacecraft crossing the mid-altitude cusp, could result from reconnection occurring simultaneously at low and high latitudes during periods of large IMF B_Y and small negative IMF B_Z.

The next panel (Plate 8, top panel) shows results for 0933 UT. Although no significant changes in the IMF direction from the previous time step are apparent, the northern merging region has moved toward lower latitudes. Its east-west direction is now more or less aligned with the Y-axis. Its latitudinal extent, however, is considerably narrower than that observed at 0931 UT. Auroral contour plots show that the region of enhanced downward flows has merged with the auroral oval and narrowed in latitude. The high-latitude band has now completely van-

ished, as expected for southward IMF. Subsequent panels in Plate 8 display the simulation results for 0934 to 0935 UT as the IMF slowly rotates back toward dusk. The change in the IMF orientation seems too small to affect significantly the global configuration of the merging regions, though a gradual broadening in latitude is perceptible when the 0933 and 0935 UT time frames are compared. The most noticeable changes occur in the auroral displays. As the IMF rotates towards dusk, flow enhancements move toward the dusk sector. In particular, a wedge-like pattern reminiscent of the earlier one at 0929 UT is apparent in the 0935 UT panel. However, in this panel the tip of the wedge points toward dusk instead of in the noon LT direction of the 0929 UT pattern. Comparison of the shape of the 0935 UT pattern with those seen in the previous frames for 0933 and 0934 UT, suggests that the wedge appears when the gradual fading of the noon region section reveals a preexisting two-banded structure, rather than from the formation of a new structure. In addition, the fact that the bands appear to fade simultaneously seems to favor the occurrence of simultaneous reconnection over a time-delay effect as an explanation for the formation of these discrete structures. However, as the IMF continues to rotate northward, the panels of Plate 2 for times 0936 and 0938 UT show that the higher latitude band remains enhanced, while the lower band fades away. This illustrates the intricacy of the processes that create these discrete structures.

Another interesting feature of the 0929–0935 UT sequence shown in Plates 7 and 8 is the strong enhancement of the downward flows seen in the Southern Hemisphere between 0931 and 0934 UT. This intensification seems to occur only when the IMF has a strong southward component. A plausible explanation of this effect is related to the sign of the B_X component of the IMF observed on June 8. As we mentioned above, open field lines from the dayside of the northern auroral region are connected to the upstream solar wind, crossing the dayside bow shock in the afternoon sector of the Southern Hemisphere. This is evident in Plate 6, and results simply from the negative B_X component of the IMF. A direct consequence of that upstream connection is that earthward flows along these open field lines are directed in the same direction (tailward) as the magnetosheath flow. In considering the open field lines from the dayside southern auroral region, it is important to keep in mind that they drape the dayside magnetosphere and are attached to the solar wind in the Northern Hemisphere, downstream of the terminator. Earthward flows along these field lines are directed sunward until they reach the Southern Hemisphere, and thus stream against the magnetosheath flow most of the time. This counter-streaming motion could explain the absence of strong downward flows in the southern auroral region during the periods of predominantly northward IMF on June 8, 2000. In obvious disagreement with that explanation is the strong enhancement of the entire dayside auroral oval of the Southern Hemisphere, which the simulation predicted would occur with the initial interaction of the interplanetary shock at 0912 UT (Plate 1). However, this seeming contradiction can be readily explained by the strong earthward plasma flow resulting from the initial pulse when it compresses the open flux tubes draping the subsolar magnetopause. Note that a

similar enhancement of the entire dayside auroral oval of the Northern Hemisphere occurs in the simulation. However, the enhancement in the Northern Hemisphere takes place one minute before the large structure displayed for time 0912 UT in Plate 1, and thus is not seen because of the 2-min sampling rate used to match IMAGE data. This scenario is consistent with the initial impact of the transmitted shock through the magnetosheath being located in the prenoon sector of the mid-latitude Northern Hemisphere.

6. Discussion

We used three-dimensional global MHD simulations to model observations of the interaction of the solar wind with the magnetosphere on June 8 and July 28, 2000. The overall results from the simulation agree very well with observations from the FUV SI-12 instrument onboard the IMAGE spacecraft. The detailed comparisons presented in Plates 1 through 4 show that the enhanced downward plasma flows into the dayside ionosphere predicted by the simulations agree remarkably well with the occurrence of dayside proton auroras observed by the imager. The dynamic pressure is high enough for magnetosheath energetic ions precipitating into the ionosphere to constitute a large fraction of the bulk of the plasma that penetrates into the magnetosphere through newly reconnected field lines. Hence, we see very good agreement with the MHD description used in the global simulation.

The simulation also does an excellent job of reproducing the dynamics of the auroral patterns observed in the IMAGES data. The June 8, 2000, 0929-0935 UT sequence described above depicts the response predicted by the global simulation for the downward flow to the back-and-forth rotation of the IMF between duskward and southward orientations. It shows a strong coupling of the azimuthal and latitudinal displacements of the auroral patterns with the B_Y and B_Z components of the IMF, respectively. These results are consistent with the FUV SI-12 images and previous observations, and clarify the relationship between the dayside proton aurora and reconnection processes at the dayside magnetopause. In addition, the simulation reveals transitional configurations characterized by auroral patterns that indicate the enhancement of the downward flow at both high latitudes and near the auroral oval. They appear as two bands making up transient wedge-like structures that appear to converge toward dusk as the IMF rotates duskward and toward noon when the IMF rotates southward. Simulations seem to indicate that these are signatures of transient simultaneous reconnection processes. Such patterns frequently occur in ground measurements and spacecraft images (e.g., Sandholt *et al.*, 1998a, b, c; Milan *et al.*, 2000) for a predominantly northward IMF with a varying B_Y. The FUV SI-12 images shown in Plates 1 and 2 display only a few of these patterns, the most prominent at 0918 and 0930 UT. However, this relative paucity might be due simply to the transient nature of these structures, and thus their observation depends on the sampling rate of the instrument and the IMF rate of change. For

AUTHOR, NEW ART WORK PLEASE

Figure 5. The picture displayed in Panel (a) is a three-dimensional rendering of the dayside magnetosphere in GSE coordinates viewed from the sun (hence dusk is located on the right and dawn on the left). The background of the picture consists of a color contour plot of the plasma beta in a cross-sectional plane (Y-Z) taken at $X = -10$ R$_E$. Superimposed over these contours, three-dimensional isosurfaces of plasma beta color-coded in red delineate the merging regions. Results of the antiparallel merging model (Crooker, 1979) are shown in Panel (b). Crooker's sketch has been rotated around the X-axis of the model to align its Z-axis with the North-South axis of the tail lobes predicted by the simulation, which point roughly in the direction of the Earth's dipole.

example, if we look only at 2-min intervals of simulation output, as displayed in Plates 1 through 4, we miss the structure occurring at time 0935 UT in Plate 8.

On a more global scale, some highly interesting results emerge from our investigation of the relationship between the topology of the dayside magnetosphere and the dynamics of proton auroras in the dayside magnetosphere. First, striking similarities exist between the merging patterns in the simulation results and those predicted by the antiparallel merging model (Crooker, 1979; Luhmann *et al.*, 1984). These similarities are evident in Figure 5, in which we compare simulation results (Panel a) with Crooker's model (Panel b). As mentioned above, the merging regions predicted by the simulation are determined by using isosurfaces of plasma beta, which are color-coded red. In addition, in Panel (b), we have rotated Crooker's sketch around the X-axis of the model in order to align its Z-axis with the North-South axis of the tail lobes, which points roughly in the direction of the Earth's dipole. One of the main consequences of that type of merging topology is that little reconnection occurs near the subsolar point. In contrast, component-merging

AUTHOR? NEW ART WORK PLEASE

Plate 1. Comparison of FUV SI-12 and simulation results for 0910 to 0924 UT on June 8, 2000. Left panels show the color contours of the corrected counts from FUV SI-12 displayed in magnetic latitude and magnetic local time coordinates. Middle panels indicate the value of the IMF clock angle in GSM coordinates, shifted in time and viewed from the tail. The right panels show in the same coordinate system, color contours of plasma flows into the ionosphere, that were predicted by the global MHD simulation. Downward flows are obtained by calculating the earthward component of the bulk flow's velocity that is parallel to the magnetic field ($V_{||}$) at the inner boundary shell of the simulation system. Both ionospheric displays are viewed from above the Northern Hemisphere.

models predict that reconnection of the Earth's field with the IMF can occur across the subsolar region for any direction of the IMF (e.g., Cowley, 1973; Gonzales and Mozer, 1974). The only constraint is that a neutral line be established such that the components of the magnetosheath and magnetospheric fields perpendicular to that neutral line are antiparallel to each other (e.g., Cowley, 1976).

An important property of the component-merging models is that they allow reconnection to occur in the subsolar region during northward IMF, as long as a significant B_Y component is present. The merging region predicted by these models is thus continuous through the subsolar point, and its orientation is determined by the B_Y component of the IMF. Hence, the merging geometries predicted by the antiparallel and component-merging models are significantly different. This is obvious for northward IMF, since the anti-parrallel model predicts reconnection will occur exclusively with the magnetotail lobe field lines downstream of the cusps. For due southward IMF ($B_Y = 0$), both models predict the merging region will lie in the equatorial plane. However, the loci of the reconnection sites predicted by the anti-parallel model diverge very quickly from the subsolar region as the

AUTHOR? NEW ART WORK PLEASE

Plate 2. Continuation of Plate 1 for 0926 to 0940 UT on June 8, 2000.

IMF B_Y (GSM) component increases (Crooker, 1979). This divergence results in a clear separation of the northern and southern merging regions for IMF with even small transverse components. In reality, the latitude gap between the two regions is probably widened by the distortion of the geomagnetic field resulting from the penetration of the B_Y component (Cowley *et al.*, 1991). At any rate, it is clear that the merging geometries seen in the simulation results for different IMF values (Plates 7 and 8) are typical of antiparallel merging. In particular, merging gaps in latitude, but not in local time, occur near the subsolar region. The divergence of the northern and southern merging regions predicted by the antiparallel merging models could also lead to significant asymmetries in the downward flows toward the ionosphere for southward IMF. Because of the relatively high-latitude locations of the reconnection sites in the pre- and post-noon regions, it is expected that in these regions magnetosheath flows determine the direction and the strength of the flows toward the ionosphere, even when the IMF has a small B_Y component. For example, for a southward IMF with a small $B_Y > 0$, the antiparallel merging model predicts that field lines threading the prenoon sector reconnect near the southern cusp (see Figure 5). Since in that region the magnetosheath flow has a large tailward component, it opposes the plasma flowing sunward from the reconnection site toward the northern ionosphere. Therefore, slower flows should be observed in the prenoon sector for southward IMF with a small $B_Y > 0$. The paucity of flows in the prenoon sector predicted by the model may explain the gap of emissions observed in that sector in the FUV SI-12 images, and to some extent in the simulation results.

AUTHOR? NEW ART WORK PLEASE

Plate 3. Results of the June 8, 2000, simulation for time 0911 UT. The snapshot is taken just after the interplanetary shock, collided with the dayside magnetopause. The (a) panels show color-coded contours of the plasma flow velocity (V_Z) plotted in a cross-sectional plane taken at $Z = 4$ R_E (GSE) and viewed from 1500 LT. Color-contours have been limited to a narrow range of velocities (± 50 km/s) to reveal the plasma flowing toward the ionosphere. The (b) panels show the same perspective as the (a) panels, but show only the field lines traced from the region of magnetospheric downward flows.

Other features emerging from the simulation are the continuity of the reconnection process and the motion of the merging regions. It is evident from the simulation results that, whatever the orientation of the IMF, reconnection takes place somewhere on the magnetopause. Although merging occurs predominantly upstream of the cusp for southward IMF and downstream of the cusp for northward IMF, merging moves continuously from one region to another as the IMF varies. Although the merging process is mostly determined by the IMF B_Z component, it is well recognized both theoretically and experimentally that the IMF B_Y component also plays a significant role by creating additional asymmetries, as these asymmetries affect both the ionospheric and magnetospheric convection systems (e.g., Khan and Cowley, 2000). As seen in the FUV SI-12 images, understanding the effects of the IMF B_Y component on the merging geometry is crucial to understanding the dynamics of the auroral region. There is also a strong effect of the IMF B_X component that is very often neglected. Although the B_X components observed remains fairly constant during the two time intervals considered in our study, the simulation indicates that Southern and Northern Hemispheres may be affected differently because of the IMF B_X component. In fact, the B_X component is very important in the dynamics of the auroral region, because it determines whether

26

AUTHOR!
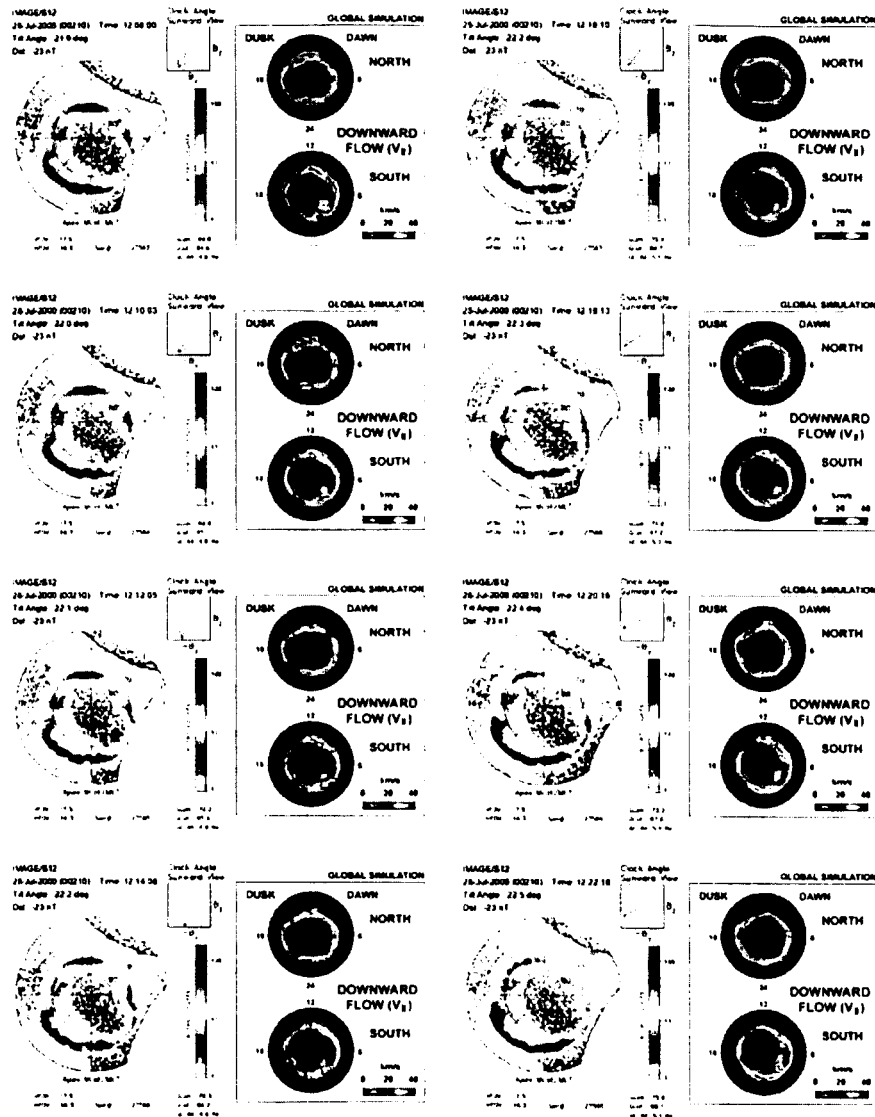Please notice that this figure
will be printed in colour!

Plate 4. Same as Plate 3, but for time 0912 UT on June 8, 2000.

AUTHOR!
Please notice that this figure
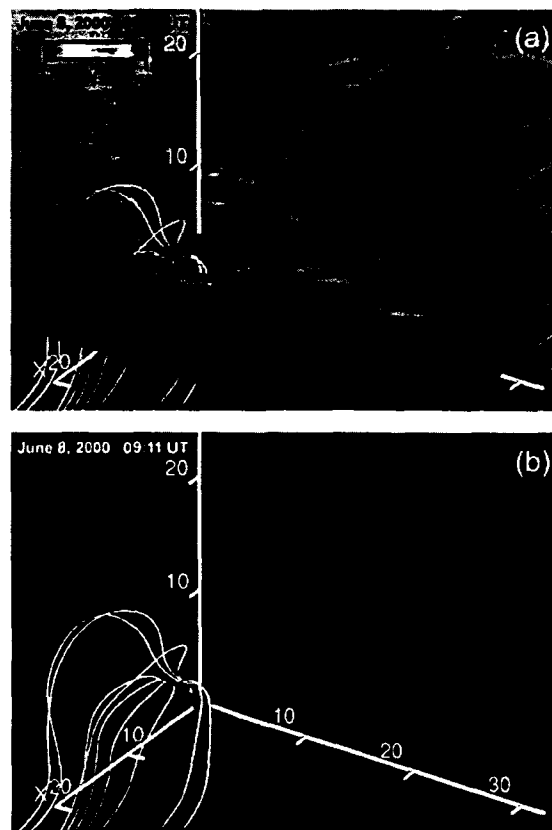**will be printed in colour!**

Plate 5. Comparison of FUV SI-12 and simulation results for 1151 to 1208 UT on July 28, 2000. The format is similar to that used in Plate 1.

open field lines are predominantly connected to the upstream or the downstream solar wind.

Furthermore, together with the B_Y component, the IMF B_X component is crucial in determining to which region of the bow shock, i.e. quasi-parallel versus quasi-perpendicular, open field lines become connected, and hence indicating the source of energetic particles penetrating the dayside auroral region (e.g., Fuselier *et al.*, 2002a). In that regard, results from the simulations indicate very interesting relationships between downward flows into the dayside auroral region and the magnetosheath plasma near the bow shock. Indeed careful inspection of Plates 7 and 8 reveals strong similarities between the shapes of plasma enhancements occurring in the magnetosheath and the auroral patterns of downward flows. A good example of that relationship can be seen in the lower panel of Plate 7 for time 0931 UT. A wedge-like pattern resembling that occurring in the auroral plot can be easily
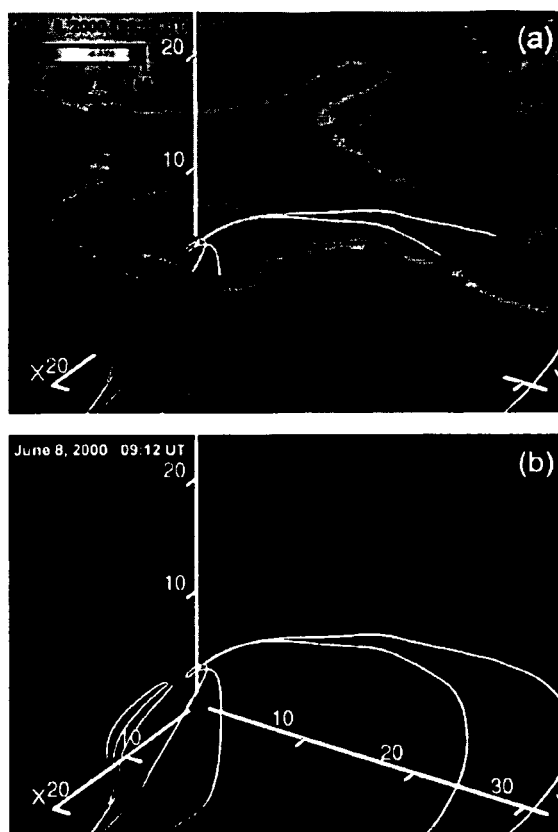
Plate 6. Continuation of Plate 5 for 1208 to 1222 UT on July 28, 2000.

identified by the red and yellow contours appearing in the upper left quadrant of the magnetosheath. It is interesting that all the panels of Plates 7 and 8 show two regions of plasma beta enhancement near the bow shock (delineated by the deep green contours), which are more or less symmetric with respect of the X-axis. Furthermore, the threading of these regions by open field lines connected to the regions of downward flows emphasizes their relation with the auroral patterns. Because the propagation speed of fast magnetosonic waves is faster across than along the magnetic field, we expect asymmetries of the Mach cone angle to be created according to the angle between the upstream velocity and the IMF (e.g., Spreiter and Stahara, 1985). A direct consequence of that process is the oblate cross section of the bow shock, with its shorter axis orthogonal to the direction of the east-west component of the IMF. Hence the shape of the bow shock and its continuous deformation as the IMF rotates, seen in Plate 7 and 8. Although these changes indicate asymmetric stresses on the magnetosheath magnetic field, cross-sectional
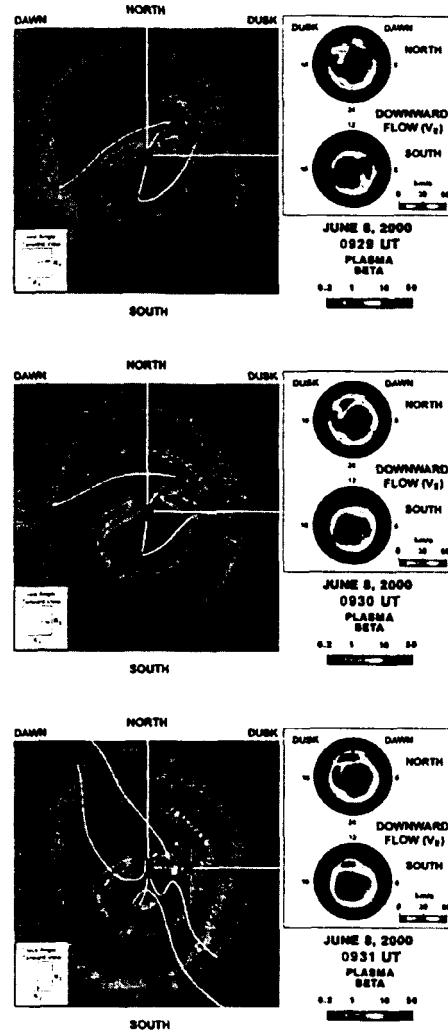
Plate 7. Each panel is composed of two subpanels showing ionospheric (right) and magnetospheric (left) results associated with the UT indicated in the lower right corner. The format for displaying the flows toward the ionosphere (framed subpanel on the right) is identical to that used in Plate 1. Middle subpanels indicate the value of the IMF clock angle in GSM coordinates, shifted in time and viewed from the Sun. The figures in the left subpanels are three-dimensional renderings of the dayside magnetosphere viewed from the sun and displayed in GSE coordinates. The background of each picture consists of a color contour plot of the plasma beta in a cross-sectional plane (Y-Z) taken at $X = -10$ R_E. Superimposed over these contours, three-dimensional isosurfaces delineate regions of plasma beta equal to 10 (color coded red), which are used to visualize merging regions in the day-side magnetosphere. Open field lines threading the regions of downward flow toward the ionosphere and high-beta plasma are displayed in yellow. These field lines establish the relation between the magnetic field merging geometry and the auroral features displayed in the right subpanels.

AUTHOR!
Please notice that this figure
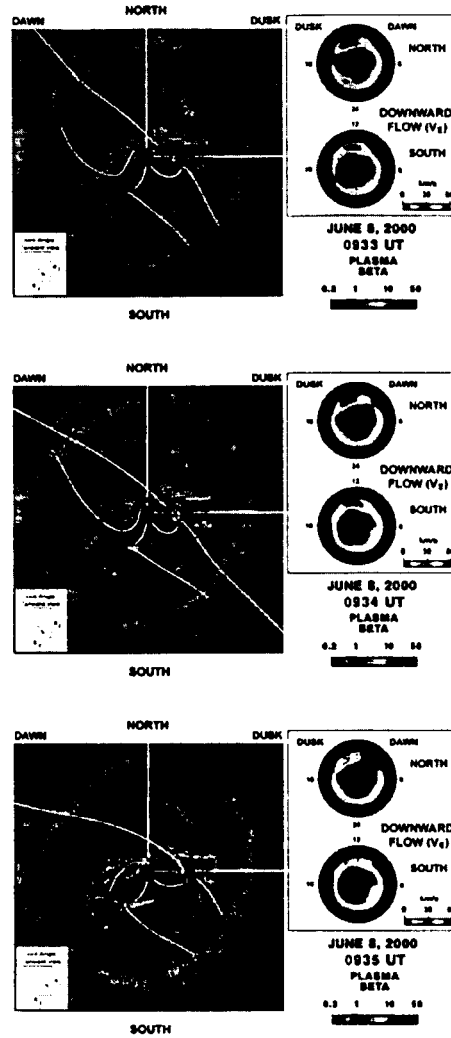will be printed in colour!

Plate 8. Continuation of Plate 7 for 0933 to 0935 UT on June 8, 2000.

plots of the plasma density show that enhancements of the plasma beta near the bow shock result from the accretion of plasma in those regions. Significant density asymmetries have been observed in the magnetosheath, though their occurrence seems to be associated with the east-west component of the IMF only near solar minimum (e.g., Paularena *et al.*, 2001). However, further investigation is needed to determine whether the effects identified in the simulations could contribute to these asymmetries. Nevertheless, as magnetosheath field lines drape around the

dayside magnetopause and compress it, newly opened field lines provide preferred channels along which the plasma in the vicinity of the magnetopause flow toward the bow shock (and the ionosphere) and locally enhance the plasma density into the reconnected tubes. As a result, cross sectional cuts through the region threaded by reconnected tubes reveal patterns similar to those made by the flow into the ionosphere.

An additional effect predicted by the global simulation is the local smearing of the merging region at low latitudes, which is seen in the upper branch of the merging regions displayed in Figure 5. This effect suggests that component merging, i.e., the occurrence of reconnection where magnetosheath field and magnetospheric field lines are not strictly antiparallel, can occur in the regions where shocked solar wind discontinuities first reach the magnetopause. The local smearing of the merging region could plausibly result from excess pressure imposed by the draping of the magnetosheath field in that region, but further investigation is needed to confirm this hypothesis. It is clear that, in addition to reproducing the clear dependence on solar wind conditions seen in the observations from the IMAGE spacecraft, the global simulations provide numerous new insights in the complex topology of the merging process occurring at the dayside magnetosphere and the intricate connection between the bow shock and the auroral region. Implications and ramifications of these processes are beyond the scope of this paper and will be reported elsewhere.

7. Summary

Enhancements in the simulated flow toward the ionosphere show a remarkable degree of agreement with proton auroras observed by the IMAGE's FUV SI-12 instrument. The global simulations accurately reproduce the strong dependence of the proton precipitation's location on the direction of the IMF. In particular, the global simulations show the poleward displacement of the precipitation when the IMF turns northward, and equatorward when the field turns southward. The simulations also reproduce very well the precipitation's azimuthal motions resulting from variations of the IMF B_Y component. These results indicate that, during the high solar wind dynamic pressure events considered, a large fraction of the magnetosheath energetic ions precipitating into the ionosphere goes toward constituting the bulk of the plasma that penetrates into the magnetosphere along newly reconnected field lines. As a result, very good agreement is achieved by using a MHD description. Global merging patterns found in the simulations agree with the antiparallel merging model, though component merging may locally broaden the merging region, especially in the region where shocked solar wind first impacts the magnetopause. The global simulations also indicate that some of the transient patterns observed by IMAGE are consistent with sporadic reconnection processes. Finally, the simulations predict the accretion of plasma near the bow

shock in the regions threaded by newly open field lines along which the flow of plasma into the dayside ionosphere is enhanced. The results of these initial comparisons between global MHD simulations and IMAGE observations emphasize the interplay between reconnection and dynamic pressure processes at the dayside magnetopause, as well as the intricate connection between the bow shock and the auroral region.

Acknowledgements

References

Berchem, J., Raeder, J., and Ashour-Abdalla, M.: 1995a, 'Reconnection at the magnetospheric boundary: Results from global magnetohydrodynamic simulation', in *Physics of the Magnetopause*, edited by Song, P., Sonnerup, B.U.Ö. and Thomsen, M.F., *Geophys. Monograph, 90*, pp. 205–213, American Geophysical Union, Washington, D.C.

Berchem, J., Raeder, J. and Ashour-Abdalla, M.: 1995b, 'Magnetic flux ropes at the high-latitude magnetopause', *Geophys. Res. Lett.* **22**, 1189.

Berchem, J., Raeder, J., Ashour-Abdalla, M., Frank, L.A., Paterson, W.R., Ackerson, L., Kokubun, S., Yamamoto, T. and Lepping, R.P.: 1998a, 'The distant tail at 200 Re: Comparison between Geotail observations and the results of a global simulation', *J. Geophys. Res.*, **103**, 9121.

Berchem, J., Raeder, J., Ashour-Abdalla, M., Frank, L.A., Paterson, W.R., Ackerson, L., Kokubun, S., Yamamoto, T. and Lepping, R.P.: 1998b, 'Large-scale dynamics of the magnetospheric boundary: Comparison between global MHD simulation results and ISTP observations', in *Encounter between Global Observations and Models in the ISTP Era*, edited by Horwitz, J., Gallager, D.L. and Peterson, W.K., *Geophys. Monograph, 104*, pp. 247–260, American Geophysical Union, Washington D.C..

Berchem, J., El-Alaoui, M. and Ashour-Abdalla, M.: 2001a, 'Modeling extreme compression of the magnetosphere: Results from a global MHD simulation of the May 4, 1998, event', in *Space Weather*, edited by Song, P., Singer, H.J. and Siscoe, G.L., *Geophys. Monograph, 125*, pp. 241–248, American Geophysical Union, Washington D.C.

Berchem, J., El-Alaoui, M. and Ashour-Abdalla, M.: 2001b, 'Consequences of the large-scale motion of the magnetospheric boundary: Results from global MHD modeling', *EOS Trans. AGU* **82**, 369.

Burch, J.L.: 1972, 'Precipitation of low-energy electrons at high latitudes: Effects of interplanetary magnetic field and dipole tilt angle', *J. Geophys. Res.* **77**, 6696.

Burch, J.L. et al.: 1985, 'IMF By-dependent plasma flow and Birkeland currents in the dayside magnetosphere, 1, Dynamics Explorer observations', *J. Geophys. Res.* **90**, 1577–1593.

Burch, J.L.: 2000, 'IMAGE mission overview, in *The IMAGE Mission*, edited by J.L. Burch, Kluwer Academic Publishers, Dordrecht', *Space Sci. Rev.* **91**, 1–14.

Carbary, J.F. and Meng, C.I.: 1986, 'Correlation of cusp latitude with Bz and AE(12) using nearly one year's data', *J. Geophys. Res.* **91**, 10047, 1986.

Collier, M.R., Slavin, J.A., Lepping, R.P., Szabo, A. and Ogilvie, K.: 1998, 'Timing accuracy for the simple planar propagation of magnetic field structure in the solar wind', *Geophys. Res. Letter* **25**, 2509.

Cowley, S.W.H.: 1973, 'A quantitative study of the reconnection between the earth's field and the interplanetary field of arbitrary orientation', *Radio Sci.* **8**, 903.

Cowley, S.W.H.: 1976, 'Comment on the merging of non-antiparallel magnetic field', *J. Geophys. Res.* **81**, 3455.

Cowley, S.W.H., Morelli, J.P. and Lockwood, M.: 1991, 'Dependence of convective flows and particle precipitation in the high-latitude ionosphere on the X and Y component of the interplanetary magnetic field', *J. Geophys. Res.* **96**, 5557.

Crooker, N.: 1979, 'Dayside merging and cusp geometry', *J. Geophys. Res.* **84**, 951.

Elphinstone, R.D., Jankowska, K., Murphree, J.D. and Cogger, L.L.: 1990, 'The configuration of the auroral distribution for interplanetary magnetic field Bz northward, 1. IMF Bx and By dependence as observed by the Viking satellite', *J. Geophys. Res.* **95**, 5791.

Escoubet, C.P., Schmidt, R., Berchem, J., Raeder, J. and Ashour-Abdalla, M.: 1997, 'Structure and dynamics of the exterior cusps: Comparison between global MHD simulations and observations', *EOS Trans. AGU* **78**, 445.

Escoubet, C.P., Berchem, J., Raeder, J., Ashour-Abdalla, M., Schmidt, R., Pedersen, A. and Fung, S.: 1998, 'The cusp observed by Polar: A statistical study and comparison with results from a global MHD model', *EOS Trans. AGU* **79**, 771.

Fedder, J.A., Slinker, S.P., Lyon, J.G. and Elphinstone, R.D.: 1995, 'Global numerical simulation of the growth phase and the expansion onset for a substorm observed by Viking', *J. Geophys. Res.* **100**, 19083.

Fox, N.J., Peredo, M. and Thompson, B.J.: 1998, 'Cradle to grave tracking of the January 6-11, 1997 Sun-Earth connection event', *Geophys. Res. Letter* **25**, 2461.

Frank, L.A., Ashour-Abdalla, M., Berchem, J., Raeder, J., Paterson, W.R., Kokubun, S., Yamamoto, T., Lepping, R.P., Coroniti, F.V., Fairfield, D.H. and Ackerson, K.L.: 1995, 'Observations of plasmas and magnetic fields in Earth's distant magnetotail: Comparison with a global MHD model', *J. Geophys. Res.* **100**, 19177.

Frey, H.U., Mende, S.B., Immel, T.J., Fuselier, S.A., Claflin, E.S., Gérard, J.-C. and Hubert, B.: 2002, 'Proton aurora in the cusp', *J. Geophys. Res.* in press.

Fuselier et al.: 2001, 'Ion outflow observed by IMAGE: Implications for source regions and heating mechanisms', *Geophys. Res. Lett.* **28**, 1163.

Fuselier, S.A., Berchem, J. and Trattner, K.J.: 2002a, 'Origins of solar wind ions in the cusp/LLBL as determined by multi-spacecraft observations and a global simulation', *J. Geophys. Res.* in press.

Fuselier, S.A., Frey, H.U., Trattner, K.J., Mende, S.B. and Burch, J.L.: 2002b, 'Cusp aurora dependence on IMF Bz', *J. Geophys. Res.* in press.

Fuselier, S.A., Mende, S.B., Moore, T.E., Frey, H.U., Petrinec, S.M., Claflin, E.S. and Collier, M.R.: 2002c, 'Cusp dynamics and ionospheric outflow', submitted to *Space Sci. Rev.*.

Gérard, J.-C, Hubert, B., Bisikalo, D.V. and Shematovitch, V.I.: 2000, 'A model of the Lyman-alpha line profile in the proton aurora', *J. Geophys. Res.* **105**, 15,795.

Goodrich, G.C., Lyon, J.G., Wiltbergere, M., Lopez, R. and Papadopoulos, K.: 1998, 'An overview of the impact of the January 10-11, 1997 magnetic cloud on the magnetosphere via global MHD', *Geophys. Res. Letter* **25**, 2537.

Gonzalez, W.D. and Mozer, F.S.: 1974, 'A quantitative model for the potential resulting from reconnection for an arbitrary interplanetary magnetic field', *J. Geophys. Res.* **79**, 4186.

Khan, H. and Cowley, S.W.H.: 2000, 'Effect of the IMF By component on the ionospheric flow overhead at EISCAT: observations and theory', *Ann. Geophysicae 18*, 1503.

Lepping, R.P., Acuna, M.H., Burlaga, L.F., Farell, W.M., Slavin, J.A., Schatten, K.H., Mariani, F., Ness, N.F., Neubauer, F.M., Whang, Y.C., Byrnes, J.B., Kennon, R.S., Panetta, P.V., Scheifele, J. and Worley, E.M.: 1995, 'The Wind magnetic field investigation', *Space Sci. Rev.* **71**, 207.

Lopez, R.E., Goodrich, C.C., Wiltberger, M., Papadapoulos, K. and Lyon, J.G.: 1998, 'Simulation of the March 9, 1995 substorm and initial comparison to data', in *Geospace Mass and Energy Flow: Results from the International Solar-Terrestrial Physics Program*, edited by Horwitz, J., Gallager, D.L. and Peterson, W.K., *Geophys. Monograph* **104**, pp. 237–245, American Geophysical Union, Washington D.C.

Luhmann, J.G. et al.: 1984, 'Patterns of potential magnetic field merging sites on the dayside magnetopause', *J. Geophys. Res.* **89**, 1739.

Lyon, J.G., Lopez, R.E., Goodrich, C.C., Wiltberger, M. and Papadapoulos, K.: 1998, 'Simulation of the March 9, 1995, substorm: Auroral brightening and the onset of lobe reconnection', *Geophys. Res. Lett.* **25**, 3039.

McComas, D.J., Blame, S.J., Barker, P., Feldman, W.C., Phillips, J.L., Riley, P. and Griffee, J.W.: 1998, 'Solar Wind Electron Proton Alpha Monitor (SWEPAM) for the Advanced Composition Explorer', *Space Science Rev.* **86**, 561.

Mende, S.B. et al.: 2000, 'Far ultraviolet imaging from the IMAGE spacecraft. 3. Spectral imaging of Lyman-alpha and OI 135.6nm, in the IMAGE Mission', edited by Burch, J.L., Kluwer Academic Publishers, Dordrecht, *Space Sci. Rev.* **91**, pp. 271–285.

Milan, S.E., Lester, M., Cowley, S.W.H. and Brittnacher, M.: 2000, 'Dayside convection and auroral morphology during an interval of northward interplanetary magnetic field' *Ann. Geophysicae* **18**, 436.

Newell, P.T. and Meng, C.-I.: 1988, 'The cusp and the cleft/boundary layer: low-altitude identification and statistical local time variation', *J. Geophys. Res.* **93**, 14549.

Newell, P.T., Meng, C.-I., Sibeck, D.G. and Lepping, R.: 1989, 'Some low-latitude cusp dependencies on the interplanetary magnetic field', *J. Geophys. Res.* **94**, 8921.

Newell, P.T. and Meng, C.-I.: 1995, 'Magnetopause dynamics as inferred from plasma observations from low-altitude satellites', in *The Physics of the Magnetopause*, edited by Song, P., Sonnerup, B.U.Ö. and Thomsen, M.F. *Geophys. Monograph Ser.* **90**, pp. 407–416, American Geophysical Union, Washington D.C.

Ogilvie, K.W. et al.: 1995, 'SWE, a comprehensive instrument for the Wind spacecraft', *Space Sci. Rev.* **71**, 55.

Onsager, T.G., Ketzing, C.A., Austin, J.B. and MacKierman, H.: 1993, 'Model of magnetosheath plasma in the magnetosphere: Cusp and mantle particles at low altitudes', *Geophys. Res. Lett.* **20**, 479.

Onsager, T.G., Scudder, J.D., Lockwood, M. and Russell, C.T.: 2001, 'Reconnection at the high-latitude magnetopause during northward interplanetary field conditions', *J. Geophys. Res*, **106**, 25,467.

Paularena, K.I., Richardson, J.D., Kolpak, M.A., Jackson, C.R. and Siscoe, G.L.: 2001, A dawn-dusk density asymmetry in Earth's magnetosheath, *J. Geophys. Res* **106**, 25,377.

Petrinec, S.M., Fuselier, S.A. and Berchem, J.: 2002, 'An examination of the magnetic merging process at the dayside magnetopause, Magnetospheric Imaging Conference', Yosemite, CA, February 2002.

Pulkinnen, T., Baker, D.N., Wiltberger, M., Goodrich, C.C., Lopez, R.E. and Lyon, J.G.: 1998, 'Pseudobreakup and substorm onset: Observations and MHD simulations compared', *J. Geophys. Res.* **103**, 14,487.

Raeder, J., Walker, R.J. and Ashour-Abdalla, M.: 1995, 'The structure of the distant geomagnetic tail during long period of northward IMF', *Geophys. Res. Lett.* **22**, 349.

Raeder, J., Berchem, J. and Ashour-Abdalla, M.: 1996, 'The importance of small scale processes in global MHD simulations: Some numerical experiments', in *Physics of Space Plasma*, edited by Chang, T. and Jasperse, J.R., vol. 14, p. 403, Cambridge, MA, MIT Center for Theoretical Geo/Cosmo Plasma Physics.

Raeder, J., Berchem, J., Ashour-Abdalla, M., Frank, L.A., Paterson, W.R., Ackerson, K.L., Kokubun, S., Yamamoto, T. and Slavin, J.A.: 1997, 'Boundary layer formation in the magnetotail: Geotail observations and comparisons with a global MHD simulation', *Geophys. Res. Lett.* **24**, 951.

Raeder, J., Berchem, J. and Ashour-Abdalla, M.: 1998, 'The Geospace Environment Modeling grand challenge: Results from a global geospace circulation model', *J. Geophys. Res.* **103**, 14,787.

Reiff, P.H. and Burch, J.L.: 1985, 'IMF By-dependent plasma flow and Birkeland currents in the dayside magnetosphere 2. A global model for northward and southward IMF', *J. Geophys. Res.* **90**, 1595.

Richmond, A.D. and Kamide, Y.: 1998, 'Mapping electrodynamic features of the high-latitude ionosphere from localized observations: Technique', *J. Geophys. Res.* **93**, 5741.

Sandholt, P.E., Farrugia, C.J., Moen, J. and Cowley, S.W.H.: 1998a, 'Dayside auroral configurations: Responses to southward and northward rotations of the interplanetary magnetic field', *J. Geophys. Res.* **103**, 20,279.

Sandholt, P.E., Farrugia, C.J., Moen, J., Cowley, S.W.H. and Lybekk, B.: 1998b, 'Dynamics of the aurora and associated convection during a cusp bifurcation event', *Geophys. Res. Lett.* **254**, 4313.

Sandholt, P.E., Farrugia, C.J., Moen, J., Noraberg, Ö., Lybekk, B., Sten, T. and Hansen, T.: 1998c, 'A classification of dayside auroral forms and activities as a function of interplanetary magnetic field orientation', *J. Geophys. Res.* **103**, 23,325.

Sato, T. and Hayashi, T.: 1979, 'Externally driven magnetic reconnection and a powerful magnetic energy converter', *Phys. Fluids* **22**, 1189.

Slinker, S.P., Fedder, J.A., Emery, B.A., Baker, K.B., Lummerzheim, D., Lyon, J.G. and Rich, J.F.: 1999, 'Comparison of global MHD simulations with AMIE simulations for the events of May 19–20, 1996', *J. Geophys. Res.* **104**, 28.

Slinker, S.P., Fedder, J.A., Ruohoniemei, J.M. and Lyon, J.G.: 2001, 'Global MHD simulation of the magnetosphere for November 24, 1996', *J. Geophys. Res.* **106**, 361.

Smith, C.W., Acuna, M.H., Burlaga, L.F., L'Heureux, J., Ness, N.F. and Scheifele, J.: 1998, 'The Ace magnetic field experiment', *Space Science Rev.* **86**, 613.

Smith, M.F. and Lockwood, M.: 1996, 'Earth magnetospheric cusps', *Rev. Geophys.* **34**, 233.

Spreiter, J.R. and Stahara, S.S.: 1985, 'Magnetohydrodynamics and gasdynamic theories for planetary bow waves', in *Collisionless Shocks in the Heliosphere: Review of Current Research*, edited by Tsurutani, B.T. and Stone, R.G., *Geophys. Monograph* **35**, pp. 85–107, American Geophysical Union, Washington, D.C.

Tsyganenko, N.A.: 1995, 'Modeling the Earth's magnetospheric magnetic field contained within a realistic magnetopause', *J. Geophys. Res.* **100**, 5599–5612.

Ugai, M.: 1985, 'Temporal evolution and propagation of a plasmoid associated with asymmetric fast reconnection', *J. Geophys. Res.* **90**, 9576.

Weiss, L.A., Reiff, P.H., Weber, E.J., Carlson, H.C., Lockwood, M. and Peteson, K.: 1995, 'Flow-aligned jet in the magnetospheric cusp: Results from the Geospace Environment Modeling pilot program', *J. Geophys. Res.* **100**, 7649.

White, W.W., Siscoe, G.L., Erickson, G.M., Kaymaz, Z., Maynard, N.C., Siebert, K.D., Sonnerup, B.U.Ö. and Weimer, D.R.: 1998, 'The magnetospheric sash and cross-tail S', *Geophys. Res. Lett.* **25**, 1605.

Wiltberger, M., Pulkkinen, T.I., Lyon, J.G. and Goodrich, C.C.: 2000, 'MHD simulation of the magnetotail during the December 10, 1996 storm', *J. Geophys. Res.* **105**, 27,649.

Wing, S., Newell, P.T. and Ruohoniemi, J.M.: 2001, 'Double cusp: Model prediction and observational verification', *J. Geophys. Res.* **106**, 25,571.

Woch, J. and Lundin, R.: 1992, 'Magnetosheath plasma precipitation in the polar cusp and its control by the interplanetary magnetic field', *J. Geophys. Res.* **97**, 1421.